Hearing Research 290 (2012) 37–44

Contents lists available at SciVerse ScienceDirect

Hearing Research

journal homepage: www.elsevier.com/locate/heares

Research paper

Temporal bone characterization and cochlear implant feasibility in the common marmoset (*Callithrix jacchus*)

Luke A. Johnson*, Charles C. Della Santina, Xiaoqin Wang

Biomedical Engineering Dept., Johns Hopkins University, 412 Traylor Research Building, 720 Rutland Avenue, Baltimore, MD 21205, USA

ARTICLE INFO

Article history:
Received 21 February 2012
Received in revised form
28 April 2012
Accepted 3 May 2012
Available online 11 May 2012

ABSTRACT

The marmoset (*Callithrix jacchus*) is a valuable non-human primate model for studying behavioral and neural mechanisms related to vocal communication. It is also well suited for investigating neural mechanisms related to cochlear implants. The purpose of this study was to characterize marmoset temporal bone anatomy and investigate the feasibility of implanting a multi-channel intracochlear electrode into the marmoset scala tympani. Micro computed tomography (microCT) was used to create high-resolution images of marmoset temporal bones. Cochlear fluid spaces, middle ear ossicles, semicircular canals and the surrounding temporal bone were reconstructed in three-dimensional space. Our results show that the marmoset cochlea is ~16.5 mm in length and has ~2.8 turns. The cross-sectional area of the scala tympani is greatest (~0.8 mm^2) at ~1.75 mm from the base of the scala, reduces to ~0.4 mm^2 at 5 mm from the base, and decreases at a constant rate for the remaining length. Interestingly, this length–area profile, when scaled 2.5 times, is similar to the scala tympani of the human cochlea. Given these dimensions, a compatible multi-channel implant electrode was identified. In a cadaveric specimen, this electrode was inserted $^3/_4$ turn into the scala tympani through a cochleostomy at ~1 mm apical to the round window. The depth of the most apical electrode band was ~8 mm. Our study provides detailed structural anatomy data for the middle and inner ear of the marmoset, and suggests the potential of the marmoset as a new non-human primate model for cochlear implant research.

1. Introduction

The marmoset monkey (*Callithrix jacchus*) is a small New World primate (300–500 g). Its hearing range and the structure of its auditory cortex are similar to other primates (Fay, 1988; de la Mothe et al., 2006; Osmanski and Wang, 2011), and it has been increasingly used as a model for investigations of central and peripheral auditory functions (Wang, 2000; Wang, 2007; Wang et al., 2008; Valero et al., 2008; Nelson and Young, 2010; Slee and Young, 2010; Bartlett et al., 2011; Watkins and Barbour, 2011). It has emerged as an important model for studying auditory processing of species-specific vocalizations (Brumm et al., 2004; Miller et al., 2009), pitch processing (Bendor and Wang, 2005, 2010) and auditory–vocal interactions (Eliades and Wang, 2003, 2005, 2008). As a non-human primate species, the marmoset shares greater similarity with humans in structural anatomy and brain organization than do feline and rodent species commonly used in cochlear implant (CI) research. Marmosets possess a rich vocal repertoire and highly communicative nature that make them well suited to studying vocal production and mechanisms related to speech processing. Moreover, there has been an increasing body of data on marmoset auditory cortical physiology (Wang et al., 1995; Liang et al., 2002; Sadagopan and Wang, 2008; Bendor and Wang, 2008), making marmoset a valuable non-human primate model to study the cortical mechanisms involved in processing CI stimulation.

The first step in developing the marmoset as a viable animal model for CI research was to study the anatomy of the temporal bone and determine the feasibility of implanting a multi-channel intracochlear electrode into its scala tympani. A detailed three-dimensional anatomical study of the marmoset temporal bone was essential for several reasons. First, there are few published data on the dimensions of the marmoset middle and inner ear structures. The number of turns of the cochlea is reported to be 2.75 (Gray, 1907; West, 1985; Borin et al., 2008). Gray (1907) and Spoor and Zonneveld (1998) reported several semicircular canal measures, and Borin et al. (2008) offered photographic documentation and qualitative description of the micro-dissection of a marmoset temporal bone, but more specific anatomical details have not been quantitatively described. As the marmoset continues to be used as a model for auditory research, dimensions of its ear

* Corresponding author. Tel.: +1 314 479 6700.
E-mail addresses: luke.johnson@jhu.edu, lukejohnson07@gmail.com (L.A. Johnson).

0378-5955/$ – see front matter © 2012 Elsevier B.V. All rights reserved.
doi:10.1016/j.heares.2012.05.002

canal, middle ear ossicles, and cochlear fluid spaces will be valuable. Second, the length, area and volume measurements of the cochlear fluid spaces described here will be useful in future modeling studies related to cochlear implants in marmosets. For example, three-dimensional reconstructions can be used in finite-element models of current flow resulting from intracochlear electric stimulation (Finley et al., 1990; Frijns et al., 1995; Hanekom, 2001; Whiten, 2007). Therefore the results from the present study serve to better establish the marmoset as a model for cochlear implant research.

Several techniques can be employed to determine cochlear dimensions. Serial histological sections can be photographed and images stacked to create three-dimensional reconstructions, but cutting large numbers of serial sections and accurately aligning images is time consuming and labor intensive. Wysocki has conducted several detailed studies of the cochlea of human, cat, dog, cattle, and macaque using latex molds (Wysocki, 1999, 2001). In his technique, liquid latex is injected into preserved temporal bones, and casts are finely sliced and direct measurements are made. Another approach is to perform high-resolution magnetic resonance imaging scans. Thorne et al. (1999) measured cochlear fluid space dimensions for human, guinea pig, bat, rat, mouse, and gerbil using three-dimensional reconstruction of MRI data. An alternative imaging approach that is less costly is X-ray micro computed tomography (microCT), which can be done at high resolution using a temporal bone specimen for characterization of volume spaces. One particular advantage is that it can be used as well for visualization of implanted electrode location (Ketten et al., 1998). We therefore chose to use high-resolution microCT scans to reconstruct the marmoset temporal bone in three-dimensional space and characterize cochlear dimensions.

2. Methods

2.1. Tissue preparation

Temporal bone specimens from five marmoset monkeys (4 adults, ages in months: 18, 45, 23, 33; 1 infant, postnatal day 7) were used in this study. Animals were euthanized with a lethal dose of Euthasol (200 mg/kg IP), or sodium pentobarbital (200 mg/kg IP), preceded by ketamine (40 mg/kg IM). Temporal bone specimens were extracted and stored in 4% paraformaldehyde solution until imaging and/or histology was conducted. Cochlea specimens ($n = 2$) used for histology after microCT imaging were decalcified for one week in 8% EDTA. Specimens were then embedded in paraffin, sectioned at 10 μm on a sled microtome and stained with H&E or toluidine blue.

2.2. MicroCT imaging and analysis

Temporal bone specimens were imaged using high resolution X-ray computed tomography (microCT) (Microphotonics, Allentown PA using SkyScan1172, Kontich, Belgium). The voxel size of the images was between 12 and 20 μm per side (cubic voxel). Image stacks were loaded into Amira software (Mercury Computer Systems, San Diego, CA) and reconstructions were made for visualization and measurements. MicroCT cross-sections were viewed in three orthogonal planes (Fig. 1a), and cochlear fluid spaces, semicircular canals and middle ear ossicles were readily identifiable. Domain reconstructions were made using a slice-by-slice selection of the region of interest (Fig. 1b). Whole specimen reconstructions were created using the *Isosurface* function in the Amira software program, which creates a surface based on a user defined pixel value threshold.

2.2.1. Characterization of cochlear fluid spaces

Soft tissue structures such as Reissner's membrane, which divides the scala media and scala vestibuli, could not be resolved in the microCT images. Therefore the scala media and scala vestibuli were grouped together as a single fluid space. Histological cross-sections were compared to the microCT images in the first two specimens processed to inform our identification of cochlear fluid spaces (Fig. 2a–c).

Length measurements were made along the lumenal axis at the center of each scala, starting at the hook region of the cochlear duct and ending at the helicotrema. Virtual cross-sections of the scala tympani and scala media/vestibuli reconstructions were made every 0.3 mm along the length of the scala. From these sections, the cross-sectional area, width and height of the fluid spaces were calculated using measuring tools available in the Amira software package. Width was measured parallel to the osseous spiral lamina where the distance between the interior and exterior wall of the scala was greatest. Height was taken at the midpoint of the cross section, perpendicular the width measurement, as shown in Fig. 2d. Fluid volumes were determined using a voxel count of the reconstructed spaces.

A top-down image of each cochlea was captured (viewed from the apex along the axis of the cochlear spiral), and the number of cochlear turns was measured relative to a reference line drawn from the beginning of the round window through the center of the cochlear spiral (Biedron et al., 2009).

2.2.2. Characterization of middle ear ossicles and semicircular canals

Marmoset middle ear ossicles (malleus, incus, and stapes) were measured as shown in Fig. 3. Dimensions measured were chosen to compare to previous characterizations of the ossicles in humans (Flohr et al., 2010; Quam and Rak, 2008; Lee et al., 2006). For the malleus, the X-axis was defined by a line connecting the tip of the short process and the top of the head. The Y-axis was defined as the line connecting the short process and the manubrium tip. M1 is the total height from the top of the head to the manubrium tip, M2 is the length of the manubrium, and M3 is the length from the lateral process to the top of the head. M4 is the angle between the two axes. For the incus, the X-axis is a line from the tip of the long process to the most prominent point on the body, and the Y-axis is a line from that point to the tip of the short process. The Z-axis is the rotational axis, and is a line from the short process tip to the external edge of the articular facet. I1 is the short process length, I2 the long process length, and I3 the angle between the X and Y axes. For the stapes, S1 is the total height and S2 and S3 are the footplate length and width respectively.

The superior, posterior and horizontal semicircular canals were also characterized. The radius of curvature R of the canal was calculated as $R = (0.5 \times [\text{height} + \text{width}]/2)$ (Spoor and Zonneveld, 1998). The height of the canal is the diameter of the canal as measured between the vestibule and the point on the canal arc (at the center of the canal lumen) that is furthest from the vestibule, and the width is the diameter of the canal measured perpendicular to the height. The total length along the midpoint of the inner side of the canal arc and vestibule was also measured; though this line does not produce a perfect circle, we term this measurement the inner circumference of the canal. The mean cross-sectional area of each canal lumen was calculated by averaging cross-sections taken every 0.4 mm along the length of each canal's thin segment.

2.3. Marmoset cochlear implantation

Our original intent was to design a cochlear implant electrode array sized according to the measured marmoset anatomy. However, we were able to identify a suitable commercially available

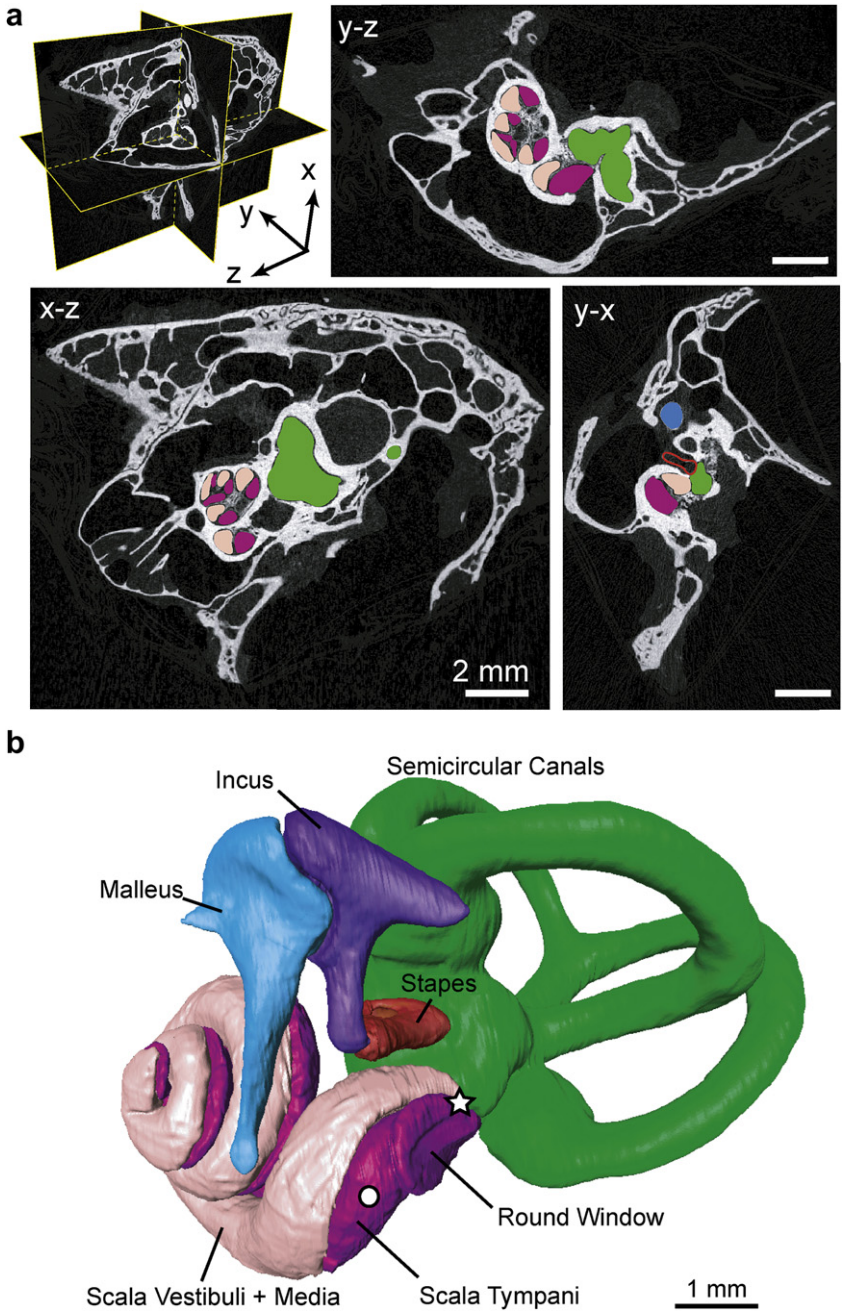

Fig. 1. MicroCT imaging of the marmoset temporal bone. (a) Specimens were imaged using high resolution X-ray computed tomography (microCT) with cubic voxel size ranging from 12 to 20 μm per side. Amira software was used to view the image stack in three orthogonal planes. Cochlear fluid spaces, middle ear ossicles and semicircular canals were identified with slice-by-slice selection of the regions of interest. Scala vestibuli and scala media were combined into a single region, as were the semicircular canals and vestibule. The scale bar is 2 mm in each cross-section. (b) Lateral view of the marmoset left inner ear. Structures were reconstructed in three-dimensional space for subsequent analysis. The white star indicates hook region of the cochlear duct, which was used as the beginning of the scala for cochlear length measurements. The white circle indicates the approximate location of cochleostomy drilled into the scala tympani for electrode insertion as described in Section 3.4.

electrode, the 10-channel Hybrid electrode (H12, Cochlear Ltd.). This electrode has a cross-sectional width of 0.4 mm and height of 0.25 mm, and cross-sectional area of 0.314 mm^2. It has 10 electrical contacts spaced evenly along the final 5.7 mm of the array. We have developed a post-auricular surgical approach for electrode implantation, similar to the approach used in human cochlear implant surgeries. In a preserved marmoset temporal bone specimen (age 17 months), a small diamond bur was used to create a cochleostomy ~1 mm anteroinferior of the round window. The electrode array was inserted into the scala tympani through the cochleostomy such that all 10 contacts of the array were inside the cochlea. Computed tomography of the specimen inserted with a cochlear implant was done at the Johns Hopkins Small Animal Imaging center using voxel size of 55 μm (Gamma Medica X-SPECT Northridge, California).

3. Results

3.1. Temporal bone reconstructions

Whole specimen reconstructions were made using a pixel value threshold and the *Isosurface* function in Amira (Fig. 4). Fig. 4 shows

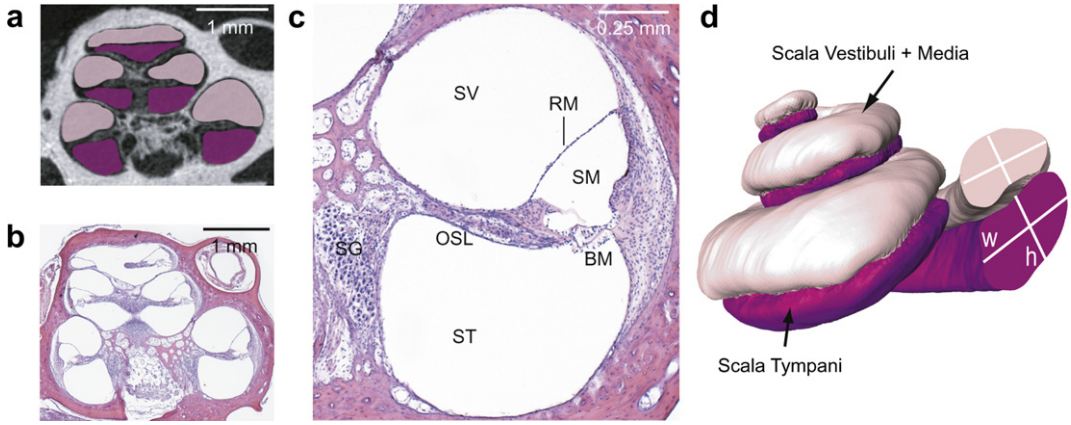

Fig. 2. Identification of cochlear fluid spaces. (a, b) MicroCT images were compared to histological sections in two specimens. This was done to instruct the demarcation of fluid spaces, since soft tissue structures were not readily visible in CT scans. (c) Radial section of the cochlear duct (higher magnification of Fig. 2b). The scala tympani (ST) was identified in microCT images using the osseous spiral lamina (OSL) as a landmark boundary for the scala vestibuli (SV). The basilar membrane (BM) boundary between the scala tympani and scala media (SM) was also not visible with microCT but assumed to be between the edge of the osseous spiral lamina and the lateral wall. Reissner's membrane (RM), which divides the scala vestibuli and scala media, was not visible with microCT, so these two spaces were combined into a single region. Spiral ganglion (SG) cells, the cell bodies of auditory nerve fibers, are visible in the cochlea modiolus in the radial section. (d) Reconstructions could be manipulated in three-dimensional spaces and virtual cross-sections could be made in any plane. Width, height, and cross-sectional area were measured every 0.3 mm along the length of the scala.

a representative reconstruction of an adult marmoset temporal bone, as well as a temporal bone reconstruction of an infant (P7) marmoset. Though skull size is smaller in the infant, the cochlea and middle ear ossicles are similar in size to the adult.

For both adults and the infant, the osseous external auditory canal was approximately 3 mm in diameter, making the marmoset a challenging species for transcanal surgical approaches such as those typically used for stapedotomy and intratympanic injection of ototoxic medications. In contrast, the adult marmoset mastoid cavity is sufficiently large that a transmastoid, trans-facial recess approach to cochlear implantation can be accomplished with only minor modifications from the technique used in humans. The main modification involves limiting depth of the initial mastoid cortex dissection to avoid injuring the horizontal semicircular canal, which can be less than 2 mm deep to the skull surface. In infant marmosets, mastoid volume is small enough that achieving

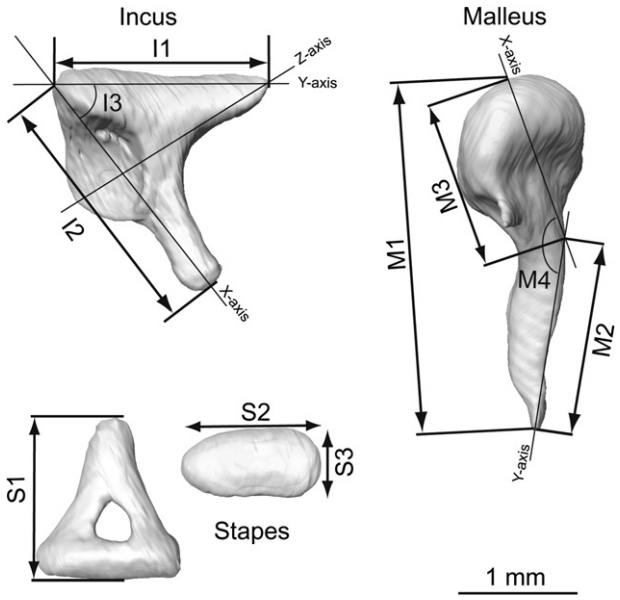

Fig. 3. Examples of reconstructions and measurements of marmoset malleus, incus and stapes. Malleus: (M1) total height from top of head to the umbo (manubrium tip), (M2) length from the umbo to end of lateral process, (M3) length from lateral process to the top of the head, (M4) angle between X and Y axes. Incus: (I1) length along the short process, (I2) length along the long process, (I3) angle between the X and Y axes. Stapes: (S1) total height of stapes, (S2) length of the footplate, (S3) width of the footplate.

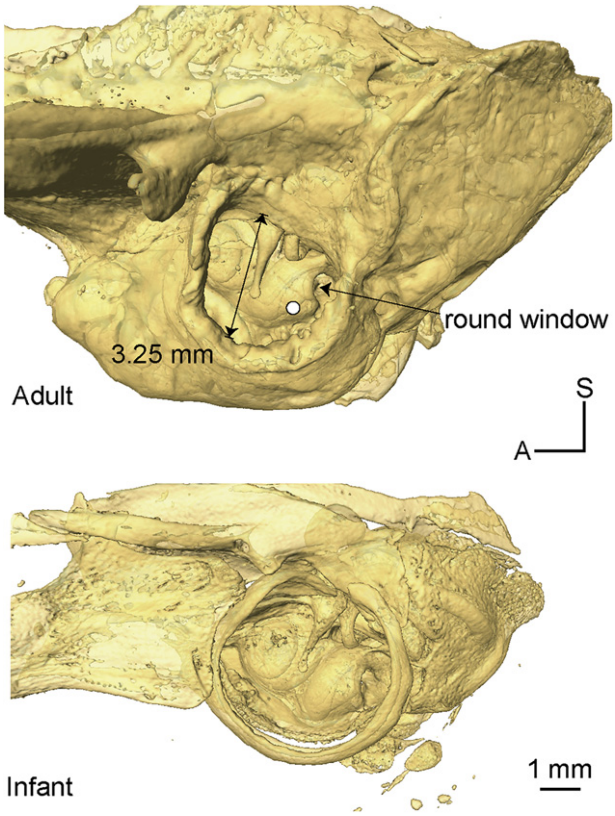

Fig. 4. Whole temporal bone specimen reconstructions from a marmoset adult (45 months) and infant (P7). Images are on the same scale. As viewed through the external ear canal, the cochlea and ossicles are visible. The white circle in the adult specimen indicates the approximate location of cochleostomy drilled into the scala tympani for electrode insertion as described in Section 3.4.

adequate access for cochlear implantation can require removal of the posterior ear canal osseous wall and temporary elevation of a tympanomeatal flap (i.e., the ear canal's periosteal lining and the tympanic membrane along with the annulus fibrosus to which it attaches). However, we have been able to maintain the ear canal soft tissue envelope, osseous ear canal wall, chorda tympani nerve and facial nerve in all adult cases.

The reconstructions could be manipulated in software and rotated to view at any angle. In the supplementary materials, a video is available for download that displays sequentially the image stack, isosurface, and reconstructions of the scala tympani, ossicles and semicircular canals. The cochlear 3-D reconstruction of one of the samples is available upon request from the author.

Supplementary video related to this article can be found at doi:10.1016/j.heares.2012.05.002.

3.2. Cochlear measurements

Cochlear fluid spaces were identified in the microCT image stack and reconstructed in three-dimensional space, as shown in Fig. 1. Since the boundary between the scala vestibuli and scala media was not well resolved, they were identified as a single fluid space. Height, width, and cross-sectional area (CSA) of the fluid spaces were measured as a function of distance along the length of the scala. The individual scala tympani CSA measurements for five marmosets are shown in Fig. 5. There was some variability between animals in scala length, which ranged from 15 to 18.3 mm, with a mean length of 16.5 and standard deviation of 1.2 mm. The scala tympani and scala vestibuli/media size profiles of the infant marmoset were within the range of the four adults, so all five were combined for subsequent analysis.

Each individual height, width and CSA profile was normalized along the length dimension to percent total length (0–100%) and scaled to the mean length of the five specimens (100% = 16.5 mm). Profiles were then averaged as shown in Fig. 6. The shaded region indicates the standard deviation about the mean. The CSA of the scala tympani is greatest at 1.75 mm from the base of the scala, measuring ~0.8 mm^2 (1.3 mm wide, 0.62 mm high), drops to ~0.4 mm^2 (0.75 mm wide, 0.6 mm high) at 5 mm from the base, and decreases at a constant rate for the remaining length. The CSA of the scala vestibuli/media reaches a maximum at 1.75 mm from the base, measuring ~0.55 mm^2 (0.94 mm wide, 0.72 mm high), and gradually decreases the remaining length of the scala. The mean (std) volume of the scala tympani was 5.22 (0.38) μl, and the mean (std) volume of the scala vestibuli/media was 5.37 (0.38) μl.

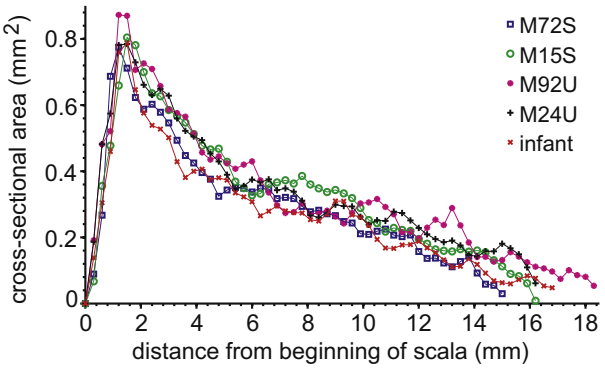

Fig. 5. Cross-sectional area of the scala tympani in 1 infant (P7) and 4 adult marmosets. Animal identification codes and ages (in months) of adult specimens: M72S (18), M15S (45), M92U (23), M24U (33).

3.3. Middle ear and semicircular canal measurements

The malleus and incus were disarticulated and damaged in one of the temporal bone specimens, so reported measurements are averages of four of the five specimens. The stapes was measured in all five specimens. The ossicle measurements of the infant fell within the range of the adult measurements, and are therefore included in the reported average. Ossicles were characterized as shown in Fig. 3, and the resulting measurements are shown in Table 1. The malleus is connected to the tympanic membrane (ear drum) along the malleus manubrium. The ear drum was faint in the CT images but visible enough to isolate in three specimens. It measured on average 4.61 mm along the length of the manubrium, and 4.71 perpendicular to the manubrium.

The semicircular canal measurements are also shown in Table 1. The horizontal canal is the smallest of the three canals, with a radius of curvature of 1.39 mm and inner circumference of 7.93 mm. It has the largest thin segment cross-sectional area of the three canals, however, at 0.23 mm^2. The posterior canal has the largest radius of curvature and inner circumference, of 1.53 mm and 8.76 mm respectively. The posterior canal cross-sectional area is 0.17 mm^2. The superior canal has a radius of curvature of 1.44 and inner circumference of 8.48 mm, and cross-sectional area of 0.19 mm^2.

Measurements of marmoset temporal bone structures including the cochlea, ossicles, ear drum and semicircular canals as described in Sections 3.1–3.3 are compiled in Table 1. The number of specimens used for the mean and standard deviation calculations are shown in parenthesis after the name of each structure.

3.4. Feasibility of cochlear implant in marmoset

Having measured marmoset cochlear dimensions, we identified an appropriate cochlear implant electrode array, the 10 channel half-band H12 electrode from Cochlear Ltd. This type of electrode was developed for clinical use in patients with residual acoustic low frequency hearing. It has smaller length and cross-sectional area than typical commercially available electrodes, which makes it well suited for use in the marmoset given its relatively small cochlea. An implanted marmoset cochlea specimen was scanned using CT to visualize insertion depth and electrode placement. Fig. 7a shows an image of the cochlea with the inserted electrode array. The array was inserted three quarters of the way around the basal turn of the scala tympani before encountering resistance. The depth of the most apical band was ~8 mm. This insertion depth matches our expectation based on scala tympani measurements. As shown in Fig. 6, the cross-sectional area of the scala tympani drops below the cross-sectional area of the electrode band (0.314 mm^2) after 8 mm in depth. To achieve a greater insertion depth in the marmoset, a smaller electrode array would be required.

The frequency-place map of the marmoset cochlea is not known, but can be roughly estimated using the Greenwood function (Greenwood, 1961). The Greenwood function is an empirically derived logarithmic relationship between frequency and its place of representation along the basilar membrane. The relationship has been shown to be consistent for many mammalian species when scaled to appropriate cochlea length and audible frequency range (Greenwood, 1990). Given cochlear spiral length of 16.5 mm from this study and an estimated marmoset audible frequency range of 125 to 36 kHz (Osmanski and Wang, 2011), we estimate that the electrodes cover a range from about 3 to 20 kHz. This frequency range would include the marmoset primary vocal range of 5–9 kHz (Pistorio et al., 2006; DiMattina and Wang, 2006; Bezerra and Souto, 2008). Fig. 7b shows the scala tympani reconstruction, indicating position from start of scala and estimated frequency representation. This result demonstrates the feasibility of

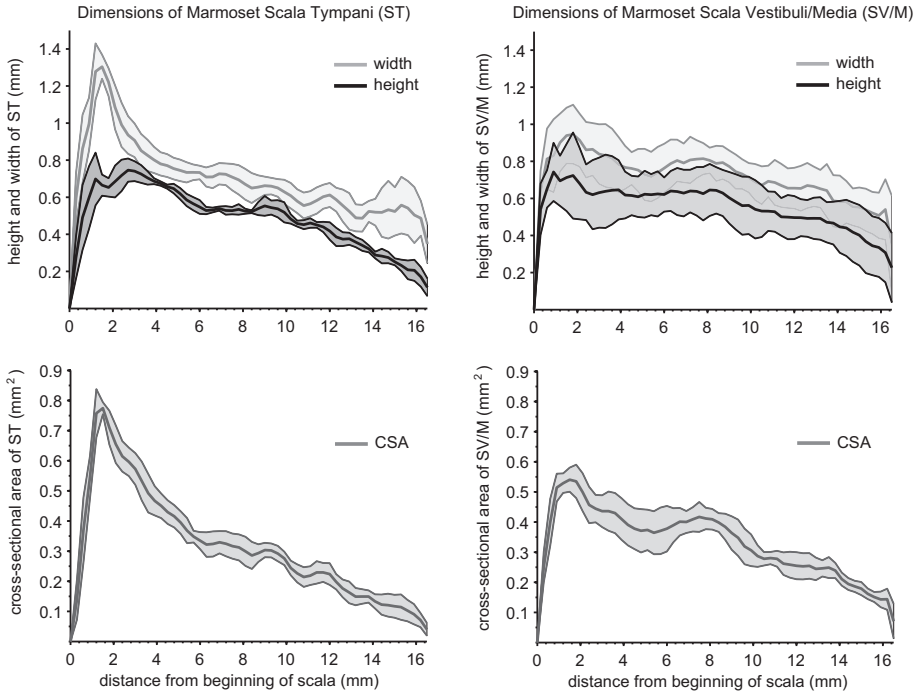

Fig. 6. Width, height and cross-sectional areas (CSA) of the marmoset cochlear fluid spaces ($n = 5$). Individual height, width and CSA profiles were scaled along the length dimension to fit the mean length of 16.5 and then averaged. The left panel shows dimensions of the scala tympani (ST), and the right panel shows dimensions of the combined scala vestibuli and scala media (SV/M). The shaded region indicates the standard deviation about the mean. The hook of the cochlear duct was defined as the beginning of the scala for distance measurements.

implanting marmosets with a multi-channel cochlear implant electrode array.

4. Discussion

In this study, marmoset temporal bone anatomy was quantitatively characterized on the basis of microCT imaging data to facilitate design of a cochlear implant array for use in marmosets. One advantage of the microCT technique is that the entire specimen volume is digitized and easily manipulated in three-dimensional space in software. Reconstructions can be viewed from any angle, virtual slices can be made, and structures can be measured without disrupting the original specimen. In contrast, histological techniques require fixation, decalcification, embedding, and sectioning, which can potentially result in shrinkage or loss of tissue. Each sample must then be photographed, imported into software and aligned in order to create 3-D reconstructions. MicroCT is typically more affordable than magnetic resonance (MR) imaging, and no special fixatives are necessary. It is possible to visualize implanted cochlear electrodes (see Fig. 7). A distinct limitation of microCT is that soft tissue structures such as Reissner's membrane are not clearly visible. It was, therefore, not possible to identify individually the scala vestibuli and scala media. However, the osseous spiral lamina projecting towards the lateral wall of the cochlea provided a reliable landmark to aid in identifying the boundary between the scala tympani and scala vestibuli and media. Our primary goals were to characterize scala tympani dimensions for the purpose of identifying an appropriate cochlear implant electrode and to visualize the inserted electrode. MicroCT was well suited for those goals.

4.1. Adult-infant temporal bone comparisons

Although the overall size of the temporal bone is larger in adults compared to the infant (see Fig. 4), the dimensions of the cochlea and ossicles of the infant were similar to those of the adults. This relationship is similar to the cochlear size comparisons between human infants and adults. In humans, there is very little postnatal growth of the cochlea and middle ear ossicles (Eby and Nadol, 1986; Dahm et al., 1993). The same is apparently true for marmosets.

4.2. Across species comparison of scala tympani dimensions

Since cochlear implant electrode arrays are implanted primarily in the scala tympani, this is the fluid space of primary interest in design of cochlear implant electrode arrays. The cross-sectional area of the scala tympani has been determined for a number of other mammalian species that have been used in cochlear implant research including human (Wysocki, 1999), macaque and cat (Wysocki, 2001), guinea pig and rat (Thorne et al., 1999). For comparative purposes, their CSA-length profiles are plotted along with the marmoset in Fig. 8.

It should be noted that the methods used for other species were different from the microCT methods reported here. The human, macaque and cat measures were taken using physical measurements of latex molds. Guinea pig and rat measures were from reconstructions using three-dimensional MRI images.

The marmoset cochlea has approximately 2.8 turns, similar to the 2.5–3 turns of the human cochlea (Biedron et al., 2009). Its CSA-length profile is quite similar to humans as well. As shown in Fig. 8, when the marmoset scala tympani CSA and length is each scaled by a factor of 2.5, the marmoset CSA-length profile is very similar to the human CSA-length profile.

4.3. Marmoset cochlear implant

A multi-channel cochlear implant electrode was inserted into the marmoset scala tympani nearly $^{3}/_{4}$ into the basal turn. Although the image reconstruction shown in Fig. 7 was from an implanted cadaveric temporal bone specimen rather than a live marmoset,

Table 1
Measurements of marmoset temporal bone structures.

Structure	Mean	Std
Cochlea ($n = 5$)		
Number of turns	2.84	0.07
Length (mm)	16.50	1.20
Scala tympani volume (μL)	5.22	0.38
Scala vestibuli/media volume (μL)	5.37	0.61
Middle ear ossicles		
Malleus ($n = 4$)		
(M1) Total height (mm)	3.22	0.18
(M2) Length from manubrium tip to end of lateral process (mm)	1.91	0.14
(M3) Length from lateral process to the end of the head (mm)	1.41	0.08
(M4) Angle between X and Y axis (degrees)	149.0	2.5
Incus ($n = 4$)		
(I1) Length along the short process (mm)	1.80	0.11
(I2) Length along the long process (mm)	2.21	0.10
(I3) Angle between short and long process (degrees)	47.0	3.0
Stapes ($n = 5$)		
(S1) Height (mm)	1.29	0.10
(S2) Length of the footplate (mm)	1.14	0.07
(S3) Width of the footplate (mm)	0.55	0.02
Ear drum (n = 3)		
Diameter along the manubrium (mm)	4.61	0.26
Diameter perpendicular to the manubrium (mm)	4.77	0.37
Semicircular canals (n = 4)		
Horizontal canal		
Radius of curvature (mm)	1.39	0.55
Mean canal cross-sectional area (mm^2)	0.23	0.05
Loop inner circumference (mm)	7.93	0.44
Posterior canal		
Radius of curvature (mm)	1.53	0.03
Mean canal cross-sectional area (mm^2)	0.17	0.01
Loop inner circumference (mm)	8.76	0.38
Superior canal		
Radius of curvature (mm)	1.44	0.05
Mean canal cross-sectional area (mm^2)	0.19	0.03
Loop inner circumference (mm)	8.48	0.08

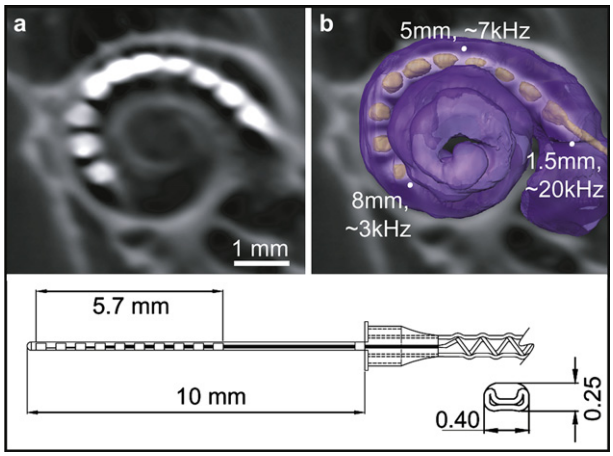

Fig. 7. Cochlear implant electrode insertion in an adult marmoset cochlea (M9R, 17 months). (a) A microCT image showing a 10 channel cochlear implant electrode (H12 Cochlear Ltd) that was inserted through a cochleostomy ~1 mm apical to the round window. (b) 3-D reconstruction of the scala tympani and electrode overlaid with the microCT cross-section. The most apical band is inserted ~8 mm, and electrodes are estimated to span a frequency-place range of 3–20 kHz. Frequency-place estimates were derived from the Greenwood function (Greenwood, 1990) scaled according to marmoset cochlear length and estimated audible frequency range (Osmanski and Wang, 2011). Electrode schematic was provided by Cochlear Ltd.

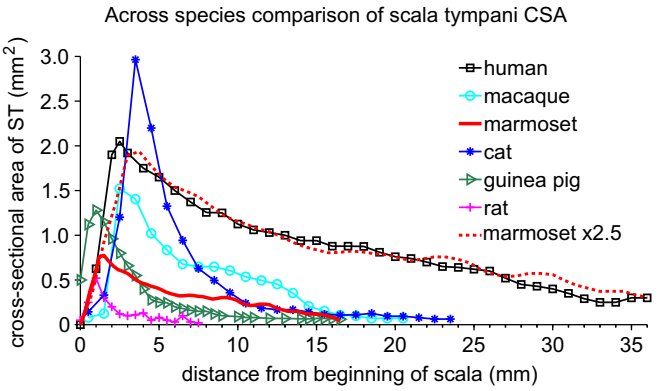

Fig. 8. Scala tympani cross-sectional area (CSA) – length profiles for several mammalian species. Human, macaque and cat dimensions are from Wysocki (1999, 2001), using a latex mold technique. Guinea pig and rat dimensions are from Thorne et al. (1999), using a MRI technique. The marmoset CSA-length profile is quite similar to human when scaling the CSA and length by a factor of 2.5.

chronic electrode implantations have now been done successfully in five marmosets in our lab, using a technique analogous to that most surgeons use for transmastoid cochlear implantation via the facial recess and a cochleostomy in humans. In this surgical approach the electrode is inserted through a cochleostomy made ~0.5–1 mm anteroinferior of (and thus apical to) the round window. This has the added benefit of permitting a somewhat deeper electrode insertion.

Our results demonstrate one of the deepest insertions of a multi-channel (>6 bands) implant electrode in an animal model (excluding humans). A comparison of cochlear turns and insertion depth in CI models is shown in Table 2. Human implant electrodes are typically inserted 1–1.75 cochlear turns (Gstoettner et al., 1999). Similarly deep insertions are possible in macaque monkeys (Shepherd et al., 1995), though macaques have not been used as a CI model for many years. Commercially available implant electrodes used in cats and guinea pigs have typically been restricted to high frequency regions (>8 kHz) in the basal ½ turn of the cochlea (Snyder et al., 2008; Fallon et al., 2009), though at least two groups have shown deeper insertion in cat cochlea with custom tapered electrode arrays (Rebscher et al., 2007; Shepherd et al., 2011). With a $^3/_4$ turn, 8 mm insertion depth, the implant should cover a frequency range from 3 to 20 kHz. This range is still considered "high frequency", but if our estimations are accurate, it should be possible to activate auditory nerve fibers that are responsive to the marmoset vocalization range of 5–9 kHz.

Table 2
Comparison of cochlear implant insertion depths across animal models.

Species	Cochlear turns	Scala tympani length (mm)	CI electrode insertion depth (# of turns)
Human	2.5–3	36	20–33 mm (1–1.75)[a]
Marmoset	2.84	16.5	~8 mm (~3/4)
Macaque	2.75	22	~10–15 mm (~1)[b]
Cat	3–3.5	23	~8 mm (~1/2–1)[c,d,e]
Guinea Pig	4	16.2	~4.5 mm (~1/2)[f]
Rat	2.2	7.2	~1.5 mm (~1/4)[g]

[a] Gstoettner et al., 1999.
[b] Shepherd et al., 1995.
[c] Fallon et al., 2009.
[d] Rebscher et al., 2007.
[e] Shepherd et al., 2011.
[f] Snyder et al., 2008.
[g] Lu et al., 2005.

4.4. Concluding remarks

This study reports the size of the marmoset scala tympani as it relates to the insertion of a multi-channel cochlear implant electrode. We also report a more complete set of measurements of marmoset temporal bone structures than has been reported previously. This includes characterization of cochlear fluid spaces, middle ear ossicles and semicircular canals. As the marmoset continues to be increasingly used as a model for auditory research, such measures will prove valuable for further comparative anatomy and modeling studies.

Acknowledgments

This work was supported by a grant from the Kleberg Foundation to X. Wang and grants from the NIH National Institute on Deafness and Other Communication Disorders (F31 DC010321 to L. Johnson and P30 DC005211 to the Center for Hearing and Balance at Johns Hopkins). We thank Haoxin Sun for assistance with Amira reconstructions of several temporal bone specimens. We also thank Zach Smith for assistance with obtaining Cochlear Ltd. electrodes, Ben Tsui and Jianhua Yu for help with CT imaging of the electrode-implanted marmoset cochlea, Jenny Estes and Nate Sotuyo for animal care, and Mohamed Lehar, Hakim Hiel and San San Yu for help with histology.

References

Bartlett, E.L., Sadagopan, S., Wang, X., 2011. Fine frequency tuning in monkey auditory cortex and thalamus. J. Neurophysiol. 106, 849–859.
Bendor, D., Wang, X., 2005. The neuronal representation of pitch in primate auditory cortex. Nature 436, 1161–1165.
Bendor, D., Wang, X., 2008. Neural response properties of primary, rostral, and rostrotemporal core fields in the auditory cortex of marmoset monkeys. J. Neurophysiol. 100, 888–906.
Bendor, D., Wang, X., 2010. Neural coding of Periodicity in marmoset auditory cortex. J. Neurophysiol. 103, 1809–1822.
Bezerra, B., Souto, A., 2008. Structure and usage of the vocal repertoire of Callithrix jacchus. Int. J. Primatol. 29, 671–701.
Biedron, S., Westhofen, M., Ilgner, J., 2009. On the number of turns in human Cochleae. Otol. Neurotol. 30, 414–417.
Borin, A., Covolan, L., Mello, L.E., Okada, D.M., Cruz, O.L.M., Testa, J.R.G., 2008. Anatomical study of a temporal bone from a non-human primate (Callithrix sp). Braz. J. Otorhinolaryngol. 74, 370–373.
Brumm, H., Voss, K., Kollmer, I., Todt, D., 2004. Acoustic communication in noise: regulation of call characteristics in a new world monkey. J. Exp. Biol. 207, 443–448.
Dahm, M.C., Shepherd, R.K., Clark, G.M., 1993. The postnatal growth of the temporal bone and its implications for cochlear implantation in children. Acta Otolaryngol. Suppl. 505, 1–39.
de la Mothe, L.A., Blumell, Suzanne, Kajikawa, Yoshinao, Hackett, Troy A., 2006. Cortical connections of the auditory cortex in marmoset monkeys: core and medial belt regions. J. Comp. Neurol. 496, 27–71.
DiMattina, C., Wang, X., 2006. Virtual vocalization stimuli for investigating neural representations of species-specific vocalizations. J. Neurophysiol. 95, 1244–1262.
Eby, T.L., Nadol, J.B., 1986. Postnatal growth of the human temporal bone. Implications for cochlear implants in children. Ann. Otol. Rhinol. Laryngol. 95, 356–364.
Eliades, S.J., Wang, X., 2003. Sensory-motor interaction in the primate auditory cortex during self-initiated vocalizations. J. Neurophysiol. 89, 2194–2207.
Eliades, S.J., Wang, X., 2005. Dynamics of auditory-vocal interaction in monkey auditory cortex. Cereb. Cortex 15, 1510–1523.
Eliades, S.J., Wang, X., 2008. Neural substrates of vocalization feedback monitoring in primate auditory cortex. Nature 453, 1102–1106.
Fallon, J.B., Shepherd, R.K., Brown, M., Irvine, D.R.F., 2009. Effects of neonatal partial deafness and chronic intracochlear electrical stimulation on auditory and electrical response characteristics in primary auditory cortex. Hear. Res. 257, 93–105.
Fay, R.R., 1988. Hearing in Vertebrates: A Psychophysics Databook. Hill-Fay Associates, Winnetka, IL.
Finley, C.C., Wilson, B.S., White, M.W., 1990. Models of neural responsiveness to electrical stimulation. In: Miller, J.M., Spelman, F.A. (Eds.), Cochlear Implants: Models of the Electrically Stimulated Ear. Springer-Verlag Inc., New York, pp. 55–96.
Flohr, S., Leckelt, J., Kierdorf, U., Kierdorf, H., 2010. How reproducibly can human ear ossicles be measured? A study of inter-observer error. Anat. Rec. 293, 2094–2106.
Frijns, J.H.M., de Snoo, S.L., Schoonhoven, R., 1995. Potential distributions and neural excitation patterns in a rotationally symmetric model of the electrically stimulated cochlea. Hear. Res. 87, 170–186.
Gray, A.A., 1907. The Labyrinth of Animals. Churchill.
Greenwood, D.D., 1961. Critical bandwidth and the frequency coordinates of the basilar membrane. J. Acoust. Soc. Am. 33, 1344–1356.
Greenwood, D.D., 1990. A cochlear frequency-position function for several species – 29 years later. J. Acoust. Soc. Am. 87, 2592–2605.
Gstoettner, W., Franz, P., Hamzavi, J., Plenk Jr., H., Baumgartner, W., Czerny, C., 1999. Intracochlear position of cochlear implant electrodes. Acta Otolaryngol. 119, 229–233.
Hanekom, T., 2001. Three-dimensional spiraling finite element model of the electrically stimulated cochlea. Ear Hear. 22, 300–315.
Ketten, D.R., Skinner, M.W., Wang, G., Vannier, M.W., Gates, G.A., Neely, J.G., 1998. In vivo measures of cochlear length and insertion depth of nucleus cochlear implant electrode arrays. Ann. Otol. Rhinol. Laryngol. Suppl. 175, 1–16.
Lee, C., Chen, P., Lee, W., Chen, J., Liu, T., 2006. Three-dimensional reconstruction and modeling of middle ear biomechanics by high-resolution computed tomography and finite element analysis. Laryngoscope 116, 711–716.
Liang, L., Lu, T., Wang, X., 2002. Neural representations of sinusoidal amplitude and frequency modulations in the primary auditory cortex of awake primates. J. Neurophysiol. 87, 2237–2261.
Lu, W., Xu, J., Shepherd, R.K., 2005. Cochlear implantation in rats: a new surgical approach. Hear. Res. 205, 115–122.
Miller, C.T., Beck, K., Meade, B., Wang, X., 2009. Antiphonal call timing in marmosets is behaviorally significant: interactive playback experiments. J. Comp. Physiol. A. Neuroethol. Sens. Neural. Behav. Physiol. 195, 783–789.
Nelson, P.C., Young, E.D., 2010. Neural correlates of context-dependent perceptual enhancement in the inferior Colliculus. J. Neurosci. 30, 6577–6587.
Osmanski, M.S., Wang, X., 2011. Measurement of absolute auditory thresholds in the common marmoset (Callithrix jacchus). Hear. Res. 277, 127–133.
Pistorio, A.L., Vintch, B., Wang, X., 2006. Acoustic analysis of vocal development in a new world primate, the common marmoset (Callithrix jacchus). J. Acoust. Soc. Am. 120, 1655–1670.
Quam, R., Rak, Y., 2008. Auditory ossicles from southwest Asian Mousterian sites. J. Hum. Evol. 54, 414–433.
Rebscher, S.J., Hetherington, A.M., Snyder, R.L., Leake, P.A., Bonham, B.H., 2007. Design and fabrication of multichannel cochlear implants for animal research. J. Neurosci. Methods 166, 1–12.
Sadagopan, S., Wang, X., 2008. Level invariant representation of sounds by populations of neurons in primary auditory cortex. J. Neurosci. 28, 3415–3426.
Shepherd, R., Verhoeven, K., Xu, J., Risi, F., Fallon, J., Wise, A., 2011. An improved cochlear implant electrode array for use in experimental studies. Hear. Res. 277, 20–27.
Shepherd, R.K., Clark, G.M., Xu, S.A., Pyman, B.C., 1995. Cochlear pathology following reimplantation of a multichannel scala tympani electrode array in the macaque. Am. J. Otol. 16, 186–199.
Slee, S.J., Young, E.D., 2010. Sound localization cues in the marmoset monkey. Hear. Res. 260, 96–108.
Snyder, R.L., Middlebrooks, J.C., Bonham, B.H., 2008. Cochlear implant electrode configuration effects on activation threshold and tonotopic selectivity. Hear. Res. 235, 23–38.
Spoor, F., Zonneveld, F., 1998. Comparative review of the human bony labyrinth. Am. J. Phys. Anthropol. Suppl. 27, 211–251.
Thorne, M., Salt, A.N., DeMott, J.E., Henson, M.M., Henson, O.W., Gewalt, S.L., 1999. Cochlear fluid space dimensions for six species derived from reconstructions of three-dimensional magnetic resonance images. Laryngoscope 109, 1661–1668.
Valero, M.D., Pasanen, E.G., McFadden, D., Ratnam, R., 2008. Distortion-product otoacoustic emissions in the common marmoset (Callithrix jacchus): parameter optimization. Hear. Res. 243, 57–68.
Wang, X., 2000. On cortical coding of vocal communication sounds in primates. Proc. Natl. Acad. Sci. U S A 97, 11843–11849.
Wang, X., 2007. Neural coding strategies in auditory cortex. Hear. Res. 229, 81–93.
Wang, X., Lu, T., Bendor, D., Bartlett, E., 2008. Neural coding of temporal information in auditory thalamus and cortex. Neuroscience 154, 294–303.
Wang, X., Merzenich, M.M., Beitel, R., Schreiner, C.E., 1995. Representation of a species-specific vocalization in the primary auditory cortex of the common marmoset: temporal and spectral characteristics. J. Neurophysiol. 74, 2685–2706.
Watkins, P.V., Barbour, D.L., 2011. Level-tuned neurons in primary auditory cortex adapt differently to loud versus soft sounds. Cereb. Cortex 21, 178–190.
West, C.D., 1985. The relationship of the spiral turns of the cochlea and the length of the basilar membrane to the range of audible frequencies in ground dwelling mammals. J. Acoust. Soc. Am. 77, 1091.
Whiten, D.M., 2007. Electro-Anatomical Models of the Cochlear Implant. PhD Thesis. Harvard-MIT Division of Health Sciences and Technology.
Wysocki, J., 1999. Dimensions of the human vestibular and tympanic scalae. Hear. Res. 135, 39–46.
Wysocki, J., 2001. Dimensions of the vestibular and tympanic scalae of the cochlea in selected mammals. Hear. Res. 161, 1–9.